

# Introducing Reactive Chemical Transport to TOUGH2: Application to Supergene Copper Enrichment

*Tianfu Xu<sup>(1)</sup>, Karsten Pruess<sup>(1)</sup>, and George Brimhall<sup>(2)</sup>*

(1) Earth Sciences Division, Lawrence Berkeley National Laboratory  
University of California, Berkeley, CA 94720

(2) Department of Geology and Geophysics  
University of California, Berkeley, CA 94720

## Introduction

Reactive chemical transport occurs in a vast variety of geochemical environments, and over a broad range of space and time scales. Different methods are available to model coupled processes of fluid flow, mass transport, and chemical reactions in subsurface systems [Yeh and Tripathi, 1989; Steefel et al., 1994; White, 1995; Lichtner et al., 1996]. These differ in their emphasis on accuracy and comprehensiveness of flow and transport modeling on the one hand, and chemical interactions between rocks and fluids on the other. Three major approaches have been used to couple mass transport and chemical reaction: (1) direct substitution approach (DSA) which substitutes the chemical reaction equations directly into the transport equations, (2) sequential iteration approach (SIA) which solves the transport and the chemical equations separately in a sequential manner with an iterative procedure, and (3) sequential non-iteration approach (SNIA) which is similar to the SIA but without the iterative procedure. The use of the DSA leads to a system of fully coupled highly nonlinear transport equations. Its advantage is high accuracy, but its main disadvantage is a very high demand on computing resources, which limits the number of species that can be handled. In the SIA and SNIA, since the sets of equations that are solved simultaneously are much smaller than in the DSA, larger systems with larger sets of chemical species can be handled. Owing to the enormous diversity of transport and chemical reaction phenomena, no universally accepted methodology for modeling such processes has emerged, or is likely to emerge. Instead, simulation methodology must be carefully chosen and tailored to the specific physical and chemical properties of the system being investigated, and to the objectives of the modeling study.

The objectives of the present work are twofold: (1) develop a general, comprehensive capability for modeling coupled processes of flow, transport, and rock-fluid interactions, and (2) develop a practical simulation tool for the study of supergene enrichment, the oxidative weathering and acidification that causes mobilization of metals in the unsaturated zone, with subsequent formation of enriched ore deposits in the reducing conditions below water table. Such redox-driven processes have produced some of the world's largest copper deposits. Redox reactions pose difficult challenges for numerical modeling because they result in huge variations in the concentrations of aqueous species involved. For example, in systems where pyrite ( $\text{FeS}_2$ ) is oxidized in the vadose zone through contact with atmospheric oxygen, aqueous oxygen concentrations may vary over 70 orders of magnitude. Similarly, between oxidizing and reducing conditions, the concentrations of sulfide and sulfite species may range over more than 90 orders of magnitude.

This paper summarizes the development for a general-purpose simulation capability for reactive chemical transport on the framework of TOUGH2 [Pruess, 1991], and its application to the one-dimensional model of supergene copper enrichment developed previously by Ague and Brimhall [1989]. This earlier effort was based on field and laboratory geochemical studies of supergene copper systems and their dynamics under conditions of climatic change [Brimhall, et al, 1985; Alpers and Brimhall, 1988 and 1989; Brimhall and Crerar, 1990] and has provided the geochemical focus for this work. By coupling the speciation and reaction path code EQ3/6 [Wolery, 1992] to TOUGH2, the code TOUGH2-EQ3/6 has comprehensive geochemical capabilities for aqueous species and secondary mineral products. TOUGH2-EQ3/6 keeps track of the full EQ3/6 chemical database for each grid block at each time step. The

process simulation capability of TOUGH2-EQ3/6 is very computationally intensive; it serves as a benchmark for the development of more efficient, approximate methods for solving field scale multi-dimensional problems of interest in hydrogeology, acid mine drainage remediation and mining engineering. For this purpose, TOUGHREACT has been developed as an alternative. This code is much more efficient (94 times faster than TOUGH2-EQ3/6 for the present problem). TOUGH2-EQ3/6 is used first for a few grid-blocks over a short time period. TOUGHREACT initially uses the speciation and secondary mineral products obtained from TOUGH2-EQ3/6. These two codes provide a comprehensive description of rock-fluid interactions during fully transient, multi-phase, nonisothermal flow and transport in hydrologically and geochemically heterogeneous media. We demonstrate application to a simplified problem of supergene enrichment of a typical copper protore that includes the sulfide minerals pyrite ( $\text{FeS}_2$ ) and chalcopyrite ( $\text{CuFeS}_2$ ).

## Methodology

Our model of flow, transport, and chemical reactions in geologic media is based on space discretization by means of integral finite differences [Narasimhan and Witherspoon, 1976]. TOUGH2-EQ3/6 code uses a non-iterative, sequential solution scheme; TOUGHREACT uses a sequential iteration approach. Both codes have the same structure (see Figure 1); full details of the mathematical and numerical model are given in [Xu et al., 1997]. The non-isothermal multiphase flow equations are solved first, and the resultant fluid velocities and phase saturations are used for transport simulation. Transport in the liquid phase is treated in terms of total dissolved concentrations. In addition, if gaseous species are present, the transport is solved in terms of their partial pressures. The resulting concentrations and partial pressures from the transport calculation are substituted into the chemical reaction module. The temperature distribution obtained from the solution of the multiphase flow equations is used to update physical and chemical parameters. The transport equations are solved on a component basis, whereas the chemical equations are solved on a grid block basis. Two time stepping levels are used. The global time step,  $\Delta t_1$ , is controlled by the solution of flow equations. During a time interval of  $\Delta t_1$ , depending on convergence, multiple steps  $\Delta t_2$ , with  $\sum \Delta t_2 = \Delta t_1$  can be used for solution of reactive transport.

## Application

A number of test cases were run for which analytical solutions are available, to verify accuracy and convergence behavior of the TOUGH2-EQ3/6 and TOUGHREACT codes. We then proceeded to the process of supergene enrichment of primary copper ores, which are exposed to oxidizing conditions over geologic time as a consequence of tectonic and climatic changes. A schematic representation of the model system is shown in Figure 2. Oxygen is supplied to a protore containing pyrite and chalcopyrite (Table 1) as a dissolved species in infiltrating rainwaters as well as by gaseous diffusion from the land surface boundary.

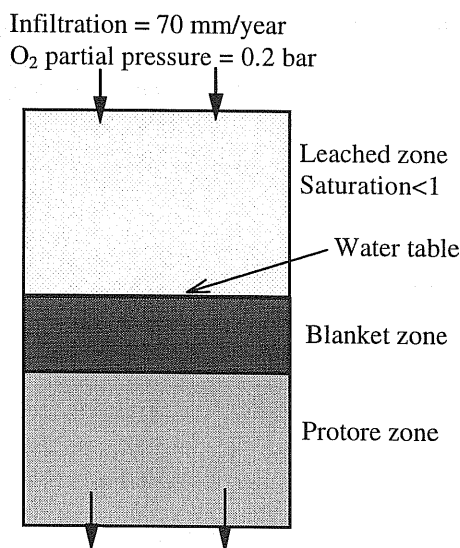


**Figure 2.** Schematic representation of a supergene enrichment system

A vertical column of 20 m thickness is used, which is discretized into 10 grid blocks with a constant spacing of 2 m. The top 5 blocks represent the unsaturated zone (water saturation: 0.43, 0.43, 0.44, 0.48, 0.72 from the top to the bottom), while the bottom 5 blocks represent the water saturated zone. A steady-state water flow regime is assumed throughout the simulation. Mineral dissolution/precipitation effects on porosity are not considered in the current simulation. A diffusion coefficient of  $4.38 \times 10^{-5} \text{ m}^2/\text{s}$  and a tortuosity of 0.1 are used for gaseous oxygen.

The column is initially filled entirely with a protore mineral assemblage as listed in Table 1. The

dissolution of the protore minerals is kinetically controlled. We use a rate expression given by Lasaga et al. [1994]:

$$r_m = k_m \sigma_m (1 - \Omega_m^\theta)^\eta \quad (1)$$

where  $m$  is the mineral index,  $r_m$  is the mineral dissolution rate (moles of mineral per unit volume of water and unit time, and negative values indicates precipitation),  $k_m$  is the rate constant (moles per unit mineral surface area and unit time) which is function of temperature,  $\sigma_m$  is the specific reactive surface area per unit fluid volume,  $\Omega_m$  is the mineral saturation ratio (i.e. the ratio between the ion activity product and the equilibrium constant). The parameters  $\theta$  and  $\eta$  must be determined from experiments; in this

simulation, they are taken equal to one. The term  $a_{H^+}^n$  accounts for the catalytic effect of  $H^+$  where the value of  $n$  is determined experimentally; in this simulation, this term is not considered. The kinetic rate constants and specific surface area are listed in Table 1. The chemical formulae of the primary minerals are given in Table 2. The mineral abundances and specific surface areas in the input data are normalized to one  $dm^3$ . The interaction of  $O_2$  gas with the aqueous solution is assumed at local equilibrium. The precipitation of secondary minerals (Table 3) during the simulation progress are considered instantaneously.

**Table 1.** Chemical properties of protore mineral reactants. Volume fraction, rate constant and specific surface area are based on Ague and Brimhall [1989] and Gerard et al. [1997]. Abundance is calculated from volume fraction (in this table) and mole volume presented in the EQ3/6 database [Wolery, 1992].

| Mineral      | Volume fraction (%) | Abundance (mol/dm <sup>3</sup> medium) | Rate constant (mol/cm <sup>2</sup> /s) | Surface area (cm <sup>2</sup> /dm <sup>3</sup> medium) |
|--------------|---------------------|--|--|--|
| Pyrite       | 9.0                 | 3.76                                   | $4.0 \times 10^{-15}$                  | 5866.7   |
| Chalcopyrite | 4.5                 | 1.05                                   | $4.0 \times 10^{-15}$                  | 5866.7   |
| Magnetite    | 4.5                 | 1.01                                   | $2.0 \times 10^{-15}$                  | 5866.7   |
| K-feldspar   | 18.0                | 1.65                                   | $3.1 \times 10^{-16}$                  | 58666.7  |
| Albite       | 9.0                 | 0.9                                    | $3.1 \times 10^{-16}$                  | 69813.4  |
| Anorthite    | 9.0                 | 0.89                                   | $1.5 \times 10^{-16}$                  | 29920.0  |
| Annite       | 4.5                 | 0.29                                   | $2.4 \times 10^{-18}$                  | 29333.3  |
| Muscovite    | 9.0                 | 0.64                                   | $2.4 \times 10^{-18}$                  | 17600.0  |
| Quartz       | 18.0                | 7.93                                   | $4.3 \times 10^{-18}$                  | 61600.1  |
| Anhydrite    | 4.5                 | 0.98                                   | $1.5 \times 10^{-16}$                  | 5866.7   |
|              | Total=90            |  |  |  |
|              | Void=10             |  |  |  |

**Table 2.** Chemical reaction equations for oxygen gas and the primary mineral reactants. The thermodynamic equilibrium constants are from the EQ3/6 database [Wolery, 1992]

| Mineral (or gas) | Reactions equation  | log K (25°C) |
|------------------|---|--------------|
| Oxygen gas       | $O_2(g) = O_2(aq)$  | -2.898       |
| Pyrite           | $FeS_2 + H_2O + 3.5O_2(aq) = 2SO_4^{2-} + Fe^{2+} + 2H^+$                         | 217.4        |
| Chalcopyrite     | $CuFeS_2 + 4O_2(aq) = 2SO_4^{2-} + Fe^{2+} + Cu^{2+}$                             | 244.07       |
| Magnetite        | $Fe_3O_4 + 8H^+ = Fe^{2+} + 2Fe^{3+} + 4H_2O$                                     | 10.4724      |
| K-feldspar       | $KAlSi_3O_8 + 4H^+ = K^+ + Al^{3+} + 3SiO_2(aq) + 2H_2O$                          | -0.2753      |
| Albite           | $NaAlSi_3O_8 + 4H^+ = Na^+ + Al^{3+} + 3SiO_2(aq) + 2H_2O$                        | 2.7645       |
| Anorthite        | $CaAl_2Si_2O_8 + 8H^+ = Ca^{2+} + 2Al^{3+} + 2SiO_2(aq) + 4H_2O$                  | 26.5780      |
| Annite           | $KFe_3AlSi_3O_{10}(OH)_2 + 10H^+ = K^+ + 3Fe^{2+} + Al^{3+} + 3SiO_2(aq) + 6H_2O$ | 29.4693      |
| Muscovite        | $KAl_3Si_3O_{10}(OH)_2 + 10H^+ = K^+ + 3Al^{3+} + 3SiO_2(aq) + 6H_2O$             | 13.5858      |
| Quartz           | $SiO_2 = SiO_2(aq)$   | -3.9993      |
| Anhydrite        | $CaSO_4 = Ca^{2+} + SO_4^{2-}$  | -4.3064      |

**Table 3.** The chemical reaction equations for secondary minerals. the thermodynamic equilibrium constants are from the EQ3/6 database [Wolery, 1992]

| Mineral                          | Reaction equation   | log K (25°C) |
|----------------------------------|---|--------------|
| Covellite                        | $\text{CuS} + \text{H}^+ = \text{Cu}^{++} + \text{HS}^-$  | 22.8310      |
| Chalcocite                       | $\text{Cu}_2\text{S} + \text{H}^+ = 2\text{Cu}^+ + \text{HS}^-$   | -34.7342     |
| Bornite                          | $\text{Cu}_5\text{FeS}_4 + 4\text{H}^+ = \text{Cu}^{++} + 4\text{Cu}^+ + \text{Fe}^{++} + 4\text{HS}^-$                           | -102.44      |
| Goethite                         | $\text{FeOOH} + 3\text{H}^+ = \text{Fe}^{+++} + 2\text{H}_2\text{O}$  | -0.283       |
| Hematite                         | $\text{Fe}_2\text{O}_3 + 6\text{H}^+ = 2\text{Fe}^{+++} + 3\text{H}_2\text{O}$  | 0.1086       |
| Kaolinite                        | $\text{Al}_2\text{Si}_2\text{O}_5(\text{OH})_4 + 6\text{H}^+ = 2\text{Al}^{+++} + 2\text{SiO}_2(\text{aq}) + 5\text{H}_2\text{O}$ | 6.8101       |
| Alunite                          | $\text{KAl}_3(\text{OH})_6(\text{SO}_4)_2 + 6\text{H}^+ = \text{K}^+ + 3\text{Al}^{+++} + 2\text{SO}_4^- + 6\text{H}_2\text{O}$   | -0.3479      |
| $\text{SiO}_2(\text{amorphous})$ | $\text{SiO}_2 = \text{SiO}_2(\text{aq})$  | -2.7136      |

A dilute oxidizing water with an oxygen fugacity (partial pressure) of 0.2 bar is initially placed in the five uppermost (unsaturated) grid blocks, while a reducing water with a fugacity of  $1.0 \times 10^{-70}$  is assumed for the remaining (saturated) grid blocks. The infiltration water composition is the same as the initial unsaturated water. TOUGH2-EQ3/6 is used first. The results of aqueous speciation and secondary mineral products are used for the subsequent TOUGHREACT simulation. A total of more than 100 species is automatically taken into account in TOUGH2-EQ3/6. However, in the TOUGHREACT simulation, only the 52 significant species are considered. The aqueous complexation is assumed at local equilibrium. Detailed results for the chemical evolution, simulated with TOUGHREACT, are given in Figures 3 and 4.

In the unsaturated zone, pyrite and chalcopyrite are oxidized and dissolved (Figure 3a). As aqueous phase oxygen is depleted through reaction with pyrite and chalcopyrite, it is replenished by dissolution from the gas phase, and diffusive transport from the atmospheric boundary at the land surface. The pH decreases downward (Figure 4a), and Cu and S concentrations increase (Figure 4d) due to pyrite and chalcopyrite oxidation. Maximum dissolved concentrations occur near the bottom of the unsaturated zone. When this water reaches the reducing saturated zone, the secondary copper bearing minerals chalcocite and covellite are precipitated (Figure 3b), forming the enrichment blanket immediately below the water table [Ague and Brimhall, 1989]. In addition, goethite precipitates in the unsaturated zone.

At the same time magnetite, K-feldspar, albite, anorthite, annite and muscovite dissolve throughout the column due to decrease of pH (Figures 3c and d). Magnetite dissolution (Figure 3a) creates additional  $\text{Fe}^{2+}$  and  $\text{Fe}^{3+}$ .  $\text{Fe}^{3+}$  acts as an oxidant, which contributes to pyrite and chalcopyrite oxidation. Dissolution of K-feldspar, albite, anorthite, annite and muscovite produces Na, K, Ca, Al and  $\text{SiO}_2(\text{aq})$ . As a result, amorphous silica or  $\text{SiO}_2(\text{am})$  precipitates throughout the column (Figure 3e). Kaolinite occurs only in the bottom 3 grid blocks of the saturated zone (Figure 3b), while alunite appears only in the top 7 grid blocks of the column (Figure 3e). There is no quartz dissolution as this mineral is stable in our simulation, as it is in nature.

## Discussion

*Quasi-stationary state.* After a brief transient evolution, the system settles into a "quasi-stationary state" (QSS; Lichtner, 1988), during which aqueous concentrations of all chemical species remain essentially constant. During QSS, dissolution of primary and precipitation of secondary minerals proceeds at constant rates. A relative concentration change and a relative dissolution (or precipitation) rate change are used to monitor attainment of QSS conditions,

$$\max_{\substack{\text{all components} \\ \text{all blocks}}} \left| \frac{C^{k+1} - C^k}{C^k} \right| < \epsilon_C \quad (2a)$$

$$\max_{\substack{\text{all minerals} \\ \text{all blocks}}} \left| \frac{r^{k+1} - r^k}{r^k} \right| < \epsilon_r \quad (2b)$$

where  $k$  is the transport time step index,  $C$  are dissolved component concentrations,  $r$  are dissolution or precipitation rates, and  $\epsilon_c$  and  $\epsilon_r$  are convergence tolerances (see Figure 5). After some 50 years relative concentration changes are reduced to  $10^{-5}$ , while dissolution rates are not very stable. The maximum relative dissolution rate changes only for the unsaturated leaching zone are shown in Figure 6. After 15 years, the rates essentially remain constant in the unsaturated zone. The observed numerical sensitivities suggest that criteria for the quasi-stationary state need to be carefully specified. This is of considerable practical importance, because substantially larger time steps should be possible during periods where a QSS is present [Neretnieks, 1997].

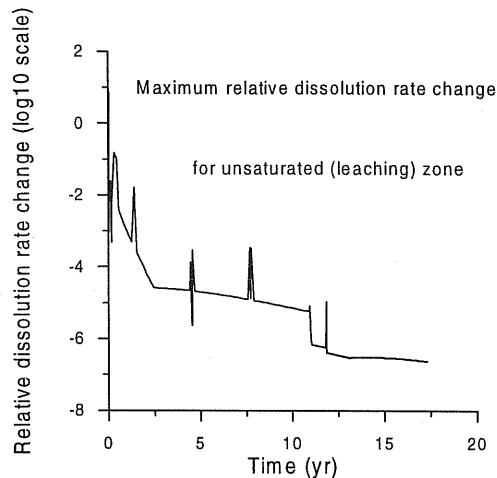


**Figure 6.** Maximum relative dissolution (precipitation) rate change for the unsaturated leaching zone.

Time step limitations. Mass balance considerations can provide useful insights into practical limitations for modeling the oxidative consumption of sulfide minerals in unsaturated flow systems. At ambient conditions of  $T = 25^\circ\text{C}$ , oxygen partial pressure  $P_{\text{O}_2} = 0.2$  bar, effective density of oxygen dissolved in water at the solubility limit is  $\rho_{\text{O}_2(l)} = 8.1 \times 10^{-3} \text{ kg/m}^3$ , while oxygen density in atmospheric air is 32 times larger, namely,  $\rho_{\text{O}_2(g)} = .258 \text{ kg/m}^3$ . Oxidation of pyrite to  $\text{Fe}^{2+}$  and  $\text{SO}_4^{2-}$  nominally requires 3.5 moles of oxygen (112 g) per mole of pyrite (120 g). A porous medium with porosity  $\phi = 10\%$  contains approximately  $8.1 \times 10^{-4} \text{ kg/m}^3$  of dissolved oxygen when the pore space is fully water-saturated, and  $2.58 \times 10^{-2} \text{ kg/m}^3$  of oxygen when completely unsaturated. The oxidation of 1 vol.% of pyrite ( $50 \text{ kg/m}^3$ ), requires 46.7 kg of oxygen per  $\text{m}^3$  of medium, which corresponds to 1,845 PV (pore volumes) of gas, or 57,654 PV of aqueous phase. In an explicit time stepping scheme, the maximum stable time step for advective flow is  $\Delta t_{\text{adv}} = \Delta x/v$ , where  $\Delta x$  is the grid spacing, and  $v$  is the advective velocity,  $v = u/\phi S$ , with  $u$  the Darcy velocity (volumetric flux), and  $S$  saturation of the flowing phase. The amount of oxygen introduced into a grid block by advective flow during the maximum stable explicit time step is

$$M_{\text{O}_2, \text{adv}} = \Delta t_{\text{adv}} u \rho_{\text{O}_2} = \Delta x \phi S \rho_{\text{O}_2} \quad (3)$$

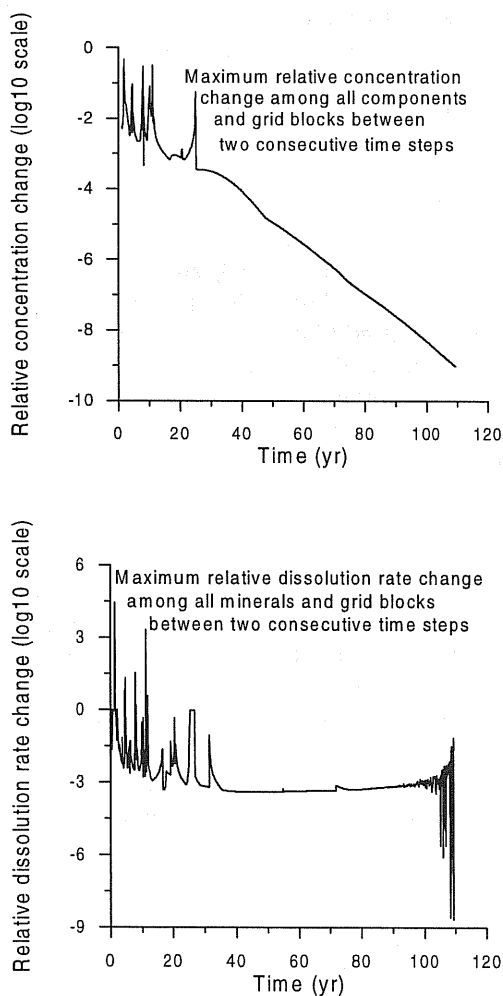


**Figure 5.** Maximum relative concentration and dissolution (precipitation) rate change for the TOUGHREACT simulation of supergene copper enrichment in a 1-D column.

which corresponds to the movement of 1 PV of fluid through the grid block. The maximum stable time step for diffusive transport is  $\Delta t_{\text{dif}} = \Delta x^2/2D_{\text{eff}}$  [Peaceman, 1977], where  $D_{\text{eff}}$  is the total effective diffusion coefficient in a porous medium under multiphase conditions. The amount of oxygen introduced into a grid block by diffusive transport during the maximum stable explicit time step is

$$M_{\text{O}_2,\text{dif}} = \Delta t_{\text{dif}} F_{\text{dif}} = \frac{\Delta x^2}{2} \nabla C \quad (4)$$

where  $F_{\text{dif}} = -D_{\text{eff}} \nabla C$  is the diffusive flux, and  $\nabla C$  is the concentration gradient driving diffusion. For the parameters used in our problem, we have  $\Delta t_{\text{adv}} = 8.64 \times 10^8$  s,  $\Delta t_{\text{dif}} = 4.56 \times 10^5$  s,  $M_{\text{adv}} = 7.29 \times 10^{-4}$  kg/m<sup>2</sup> and  $M_{\text{dif}} = 0.517$  kg/m<sup>2</sup>. The amount of oxygen that can be supplied during an explicit time step is seen to be small, suggesting that for modeling of "substantial" reaction progress, an explicit time stepping approach is impractical for advectively dominated conditions, and may at best be marginally viable for diffusively dominated conditions. The fully implicit simultaneous solution is not an attractive alternative either, because of the large number of species conservation equations that need to be solved (of order of 100 per grid block in our problem). The most promising approach appears to be a "mixed explicit-implicit" or "adaptive implicit" scheme [Evans et al., 1954; Thomas, 1982], where grid blocks are dynamically "switched" from explicit to implicit time stepping in the course of a simulation, based on their intrinsic time step constraints. Such an approach would seem well suited for our problem: in regions where oxygen consumption is strong, many chemical species will be present, but time step constraints are relaxed so that an explicit approach should be effective; in regions where oxygen-consuming minerals have been depleted we have the opposite characteristics: explicit time step constraints are severe, implicit time stepping is favored and seems practical because only a limited number of chemical species is active.

## Conclusions and future work

Oxidative weathering is an extremely difficult process to model numerically, because (1) it is driven by oxygen whose concentration in ambient soil gas, and dissolved in pore water in the unsaturated zone, is very small compared to the amounts of solid

minerals which are to be reacted, and (2) the chemical activities and total elemental solubilities of key species vary over an enormous range of tens of orders of magnitude during redox processes. We have presented a sequential approach for modeling flow, transport, and chemical reactions, and have explored a non-iterative (TOUGH-EQ3/6) and an iterative (TOUGHREACT) solution scheme. Our model provides a comprehensive suite of process modeling capabilities. An application to a supergene copper enrichment system demonstrated results reasonably close to known geochemical behavior. Mass balance and time stepping considerations showed that explicit time-stepping approaches can only be used for modeling "incremental" evolution of redox-driven systems over brief time periods. In order to simulate substantial reaction process and mobilization and reprecipitation of large amounts of chemical species over geologic time, one should benefit from the quasi-stationary approximation. Alternatively it will be necessary to resort to mixed explicit-implicit or fully implicit methods.

## Acknowledgement

The authors appreciate stimulating discussions with Tom Wolery, John Apps, and Frederic Gérard. We thank Eric Sonnenthal and Nicolas Spycher for their careful review of the manuscript. This work was supported by the Laboratory Directed Research and Development Program of the Ernest Orlando Lawrence Berkeley National Laboratory, under Contract No. DE-AC03-76SF00098 with the U.S. Department of Energy.

## References

- Ague, J. J., and Brimhall G. H., Geochemical modeling of steady state and chemical reaction during supergene enrichment of porphyry copper deposits, *Econ. Geol.*, 84, 506-528, 1989.
- Alpers, C.N. and Brimhall, G.H., Middle Miocene climatic change in the Atacama Desert, northern Chile: Evidence from supergene mineralization at La Escondida: *Geol. Soc. Amer. Bull.*, v. 100, p. 1640-1656, 1988.
- Alpers, C.N. and Brimhall, G.H., Paleohydrologic evolution and geochemical dynamics of cumulative supergene metal enrichment at La Escondida, Atacama Desert, northern Chile: *Econ. Geol.*, v. 84, p. 229-255, 1989.
- Brimhall, G.H., Alpers, C.N. and Cunnigham, A.B., Analysis of supergene ore-forming processes and ground water solute transport using mass balance principles, *Econ. Geol.*, v. 80, p. 1227-1256, 1985.

- Brimhall, G.H. and Crerar, D.A., Ore fluids: Magmatic to supergene, in *Thermodynamic Modeling of Geological Materials: Minerals, Fluids and Melts*, I. Carmichael and H. Eugster, eds., Min. Soc. Amer. Reviews in Mineralogy, v. 17, ch. 10, p. 235-321, 1990.
- Gérard, F., T. Xu, G. Brimhall and K. Pruess, Modeling reactive chemical transport problems with the codes EQ3/6 and TRANQUI, Lawrence Berkeley Laboratory Report LBL-40505, Berkeley, California, 1997.
- Evans, G.W., R.J. Brousseau and R. Keirstead. Instability Considerations for Various Difference Equations Derived from the Diffusion Equation, Lawrence Livermore National Laboratory Report UCRL-4476, Livermore, CA, 1954.
- Lasaga, A. C., Soler, J. M., Ganor, J., Burch, T. E., and K. L. Nagy, Chemical weathering rate laws and global geochemical cycles, *Geochim. Cosmochim. Acta*, 58, 2361-2386, 1994.
- Lichtner, P.C. The Quasi-Stationary State Approximation to Coupled Mass Transport and Fluid-Rock Interaction in a Porous Medium, *Geochim. Cosmochim. Acta*, Vol. 52, pp. 143 - 165, 1988.
- Lichtner, P.C., C.I. Steefel and E.H. Oelkers. Reactive Transport in Porous Media, *Rev. in Mineralogy*, Vol. 34, Mineralogical Society of America, Washington, DC, 1996.
- Narasimhan, T. N. and P. A. Witherspoon. An Integrated Finite Difference Method for Analyzing Fluid Flow in Porous Media, *Water Res. Res.*, 12 (1), 57-64, 1976.
- Neretnieks, I., J.W. Yu and J. Liu. An Efficient Time Scaling Technique for Coupled Geochemical and Transport Models, *J. Contam. Hydr.*, Vol. 26, pp. 269 - 277, 1997.
- Peaceman, D. W. *Fundamentals of Numerical Reservoir Simulation*, Elsevier, Amsterdam, The Netherlands, 1977.
- Pruess, K. TOUGH2 - A General Purpose Numerical Simulator for Multiphase Fluid and Heat Flow, Lawrence Berkeley Laboratory Report LBL-29400, Lawrence Berkeley Laboratory, Berkeley, CA, May 1991.
- Steefel, C. I., and A. C. Lasaga, A coupled model for transport of multiple chemical species and kinetic precipitation / dissolution reactions with applications to reactive flow in single phase hydrothermal system, *Am. J. Sci.*, 294, 529-592, 1994.
- Thomas, G.W. *Principles of Hydrocarbon Reservoir Simulation*. International Human Resources Development Corporation, Boston, 1982.
- White, S.P. Multiphase Non-Isothermal Transport of Systems of Reacting Chemicals, *Water Resour. Res.*, Vol. 32, No. 7, pp. 1761-1772, 1995.
- Wolery, T. EQ3/6, A Software Package for Geochemical Modeling of Aqueous Systems: Package Overview and Installation Guide (Version 7.0), Lawrence Livermore National Laboratory Report UCRL-MA-110662 PT1, Livermore, CA 94550, September 1992.
- Xu, T., F. Gérard, K. Pruess and G. Brimhall, Modeling non-isothermal multiphase multi-species reactive chemical transport in geologic media, Lawrence Berkeley Laboratory Report LBL-40504, Berkeley, California, 1997.
- Yeh, G.T. and V.S. Tripathi. A Critical Evaluation of Recent Developments in Hydrogeochemical Transport Models of Reactive Multichemical Components. *Water Resour. Res.*, Vol. 25, No. 1, pp. 93 - 108, 1989.

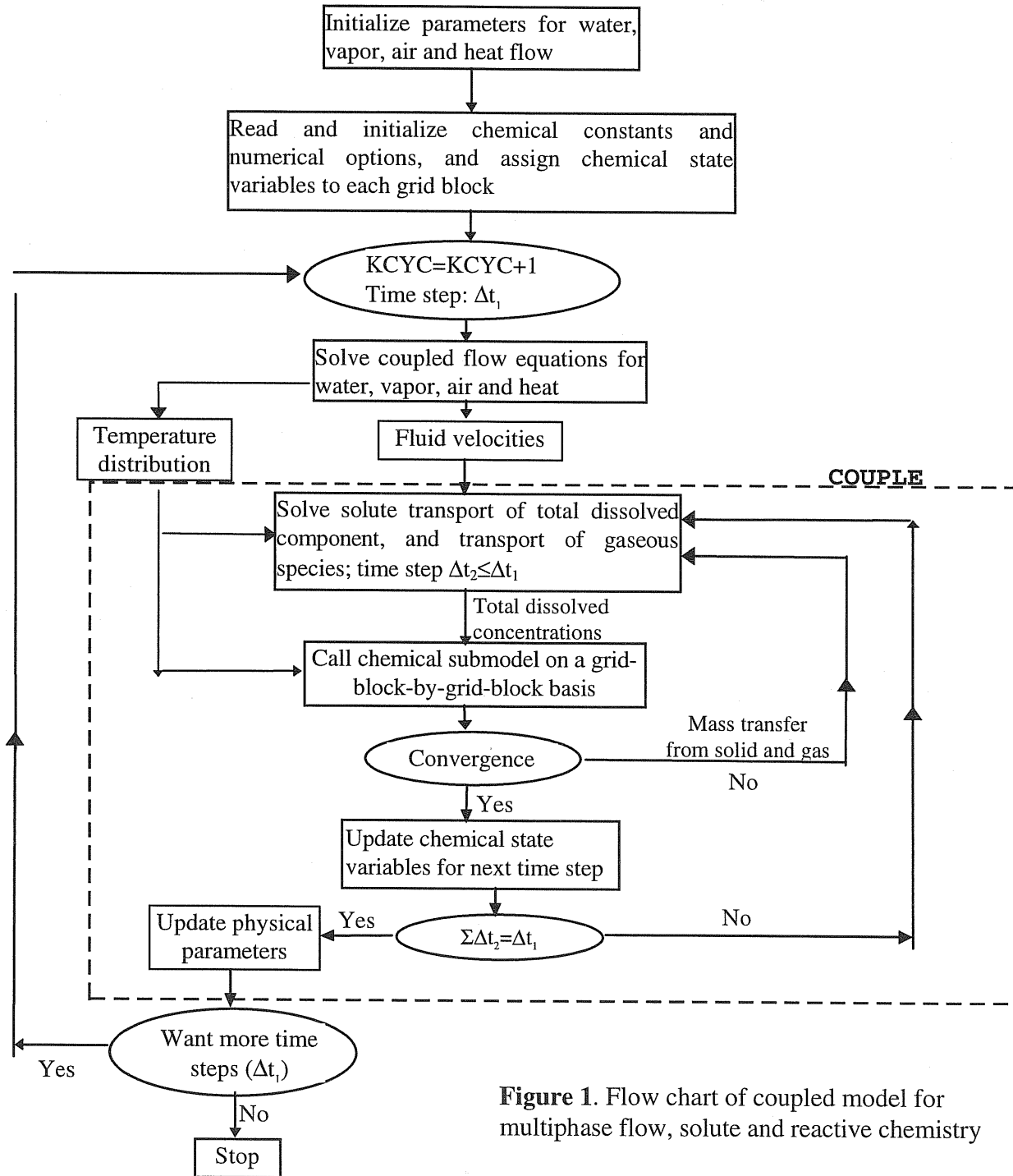
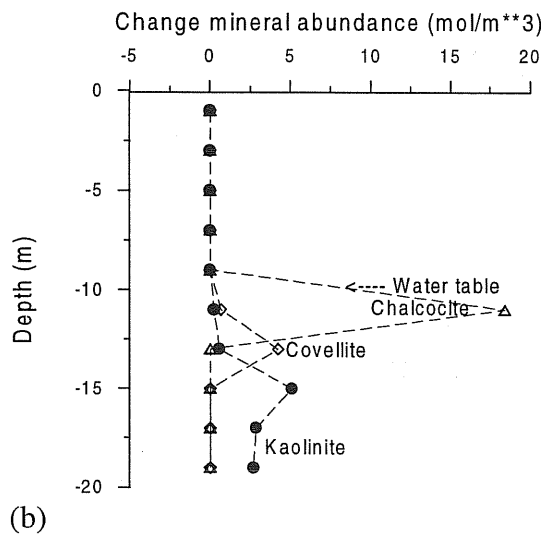
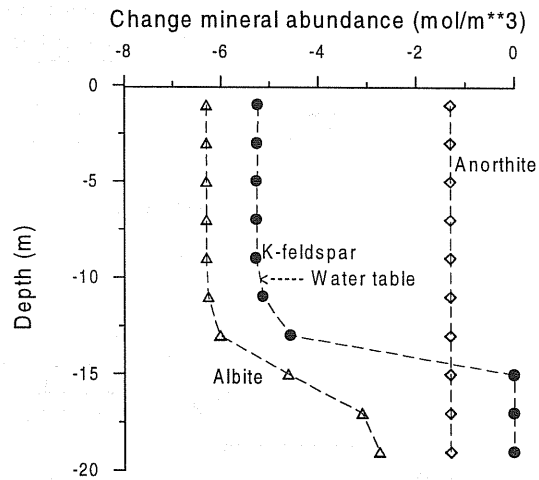
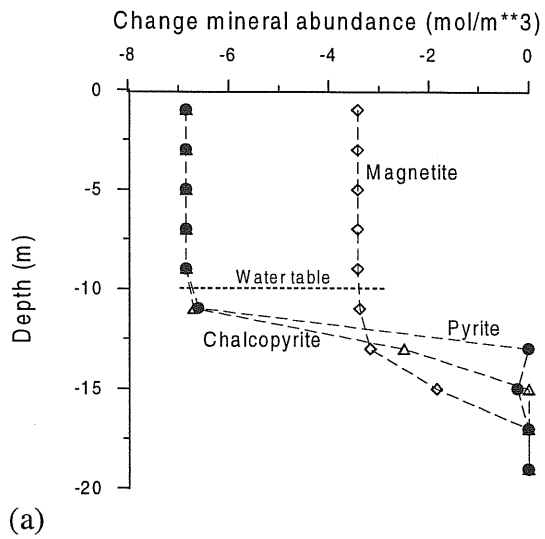
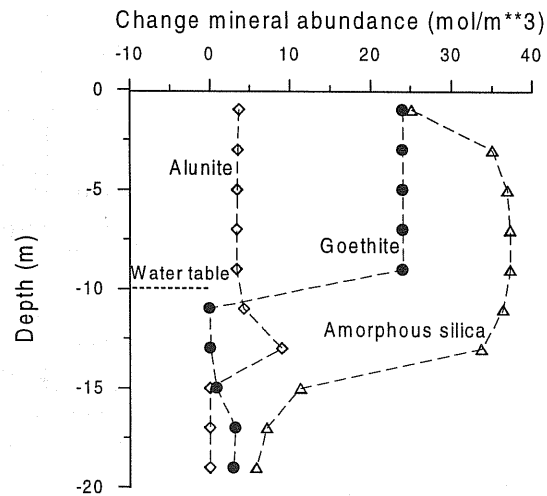


**Figure 1.** Flow chart of coupled model for multiphase flow, solute and reactive chemistry



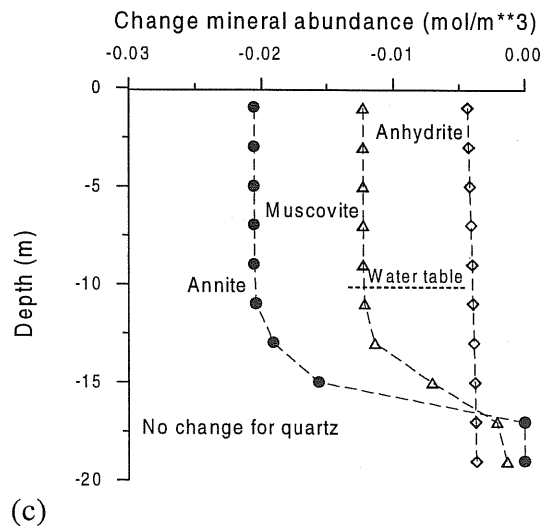


(d)



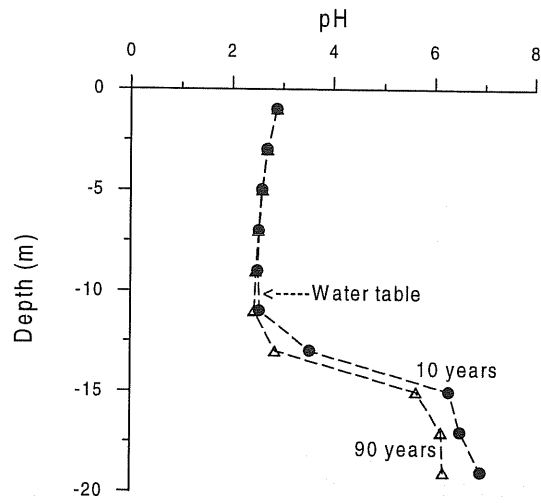
(b)

(e)

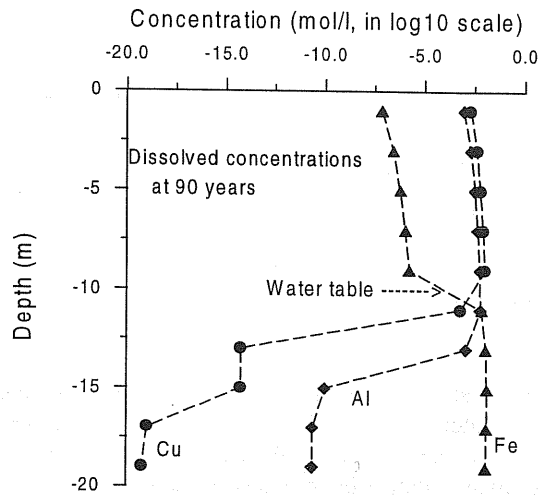


(c)

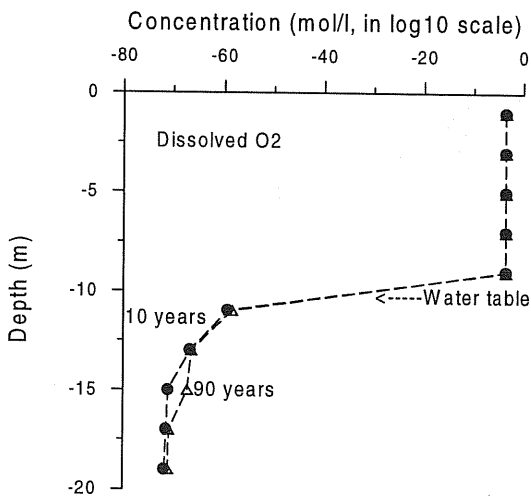
**Figure 3.** Change of mineral abundances (in moles per cubic meter medium) after 90 years. Negative values indicate dissolution, positive indicate precipitation.



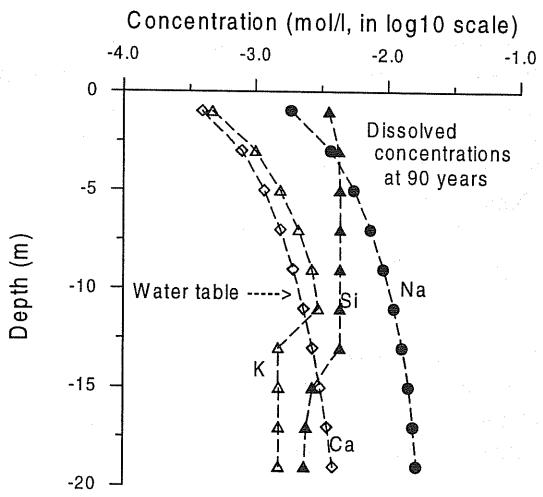
(a)



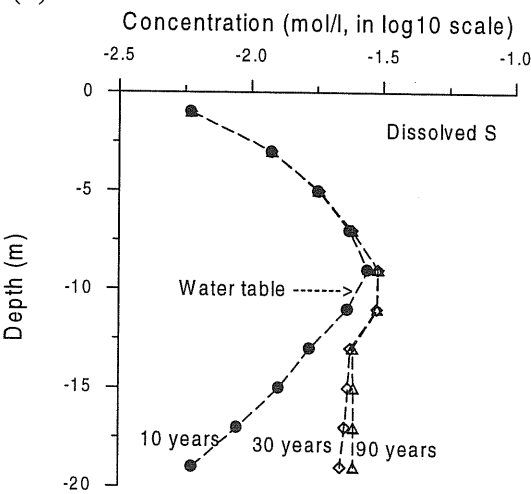
(d)



(b)



(e)



(c)

**Figure 4.** Total dissolved concentration distribution along the vertical column.